WILEY
Aggregate
Open Access

RESEARCH ARTICLE OPEN ACCESS

Dual-Mediated Aggregate Electrochemiluminescence of Rubrene

Li Dai[1,2,3] | Tong Jiang[1] | Baotao Kang[1] | Yu Du[1] | Zhongfeng Gao[1] | Xiang Ren[1] | Dan Wu[1] | Hongmin Ma[1] | Qin Wei[1] | Huangxian Ju[1,4]

[1]Key Laboratory of Interfacial Reaction & Sensing Analysis in Universities of Shandong, Collaborative Innovation Center for Green Chemical Manufacturing and Accurate Detection, School of Chemistry and Chemical Engineering, University of Jinan, Jinan, China | [2]Department of Nephrology, The First Affiliated Hospital of Zhejiang Chinese Medical University, Zhejiang Provincial Hospital of Traditional Chinese Medicine, Hangzhou, China | [3]Institute of Analytical Chemistry, Department of Chemistry, Zhejiang University, Hangzhou, China | [4]State Key Laboratory of Analytical Chemistry for Life Science, School of Chemistry and Chemical Engineering, Nanjing University, Nanjing, China

Correspondence: Hongmin Ma (chm_mahm@ujn.edu.cn) | Qin Wei (sdjndxwq@163.com) | Huangxian Ju (hxju@nju.edu.cn)

Received: 15 January 2026 | **Revised:** 11 February 2026 | **Accepted:** 20 February 2026

Keywords: electrochemiluminescence | hole-transporting | microfluidic chips | nanoaggregates

ABSTRACT

Electrochemiluminescence (ECL) populates the luminescent excited states through electrochemical reactions. It is challenging to mediate the ECL behaviors of molecular nanoaggregates because both the photophysical and electrochemical properties usually deteriorate in aggregate states. In this work, we demonstrate an unprecedented supramolecular strategy that simultaneously modulates both the photophysical and electrochemical factors governing ECL. The ECL performance of rubrene (RUB) nanoaggregates can be significantly enhanced through the incorporation of hole-transporting molecules as both redox and photophysical mediators. A balanced state, inhibiting the singlet fission (SF) and retaining the triplet–triplet annihilation (TTA), was achieved for RUB, which not only reduced the quenching of luminescent singlet state excitons but also well utilized the electrochemically generated triplet state excitons. The redox-mediating properties of hole-transporting molecules toward co-reactant not only promote the formation of excitons but also reduce the luminescent potential. The RUB nanoaggregates showed significantly enhanced photoluminescence quantum efficiency (2.3-fold) and ECL intensity (50-fold) in aqueous conditions and were demonstrated as promising ECL imaging probes. This work opens up a new avenue for the preparation of ECL nano-emitters with high-brightness in aqueous conditions.

1 | Introduction

Electrochemiluminescence (ECL), also known as electrogenerated chemiluminescence or electrochemical luminescence, is a promising analytical method combining the high sensitivity of chemiluminescence with the controllability of electrochemistry [1]. ECL has been widely used in commercial bioanalysis and has found several new attractive applications [2], such as ECL microscopy [3]. While these achievements are still confined to the use of coordination complex probes of noble metals (Ru and Ir), the exploitation of alternative luminophores with high efficiency and low-cost is a main focus for the development of ECL techniques [4, 5].

Although various types of materials, especially nanostructured particles [6, 7], have been proposed as state-of-the-art luminophores, the construction of ECL probes with good compatibility in aqueous conditions remains a great challenge. Due to the narrow electrochemical window of water, the probes and the co-reactants must possess sufficiently low redox potentials

to generate radical ions [8, 9], which subsequently undergo annihilation to populate the excited state [10]. Regarding the photophysical properties of luminophores, exciton management is equally crucial [11]. Similar to the concerns of internal quantum efficiency (IQE) in organic light-emitting diode (OLED), efficient utilization of triplet excitons through effective spin-state manipulation is crucial for achieving high-efficiency ECL systems [12]. The strategies for harvesting triplet excitons in ECL systems include the development of luminophores with room-temperature phosphorescence (RTP) [13] or thermally activated delayed fluorescence (TADF) [14, 15]. However, these long-lived triplet excitons face tremendous oxygen quenching [16], which is inherently difficult to prevent in aqueous conditions. Triplet–triplet annihilation (TTA) is another consideration for the utilization of triplet excitons. In contrast, the triplet excitons in TTA systems exhibit relatively short lifetimes, which enhance their tolerance to oxygen quenching [17].

Due to the unique electronic structure, rubrene (RUB) has been well exploited as a TTA material in the field of optoelectronics [18, 19]. Actually, RUB is one of the earliest reported ECL luminophores, and the contribution of TTA to the ECL emission has also been confirmed [20]. Nevertheless, the poor water solubility of RUB restricts its application in bioanalysis, which is always conducted in aqueous conditions [21]. We have previously demonstrated that small nanoaggregates (NAs) of pure organic molecules show promising potential in aqueous conditions [22]. Unfortunately, singlet fission (SF) rather than TTA dominates the exciton process in the aggregated states of RUB, resulting in low luminescence quantum efficiency. We have also demonstrated that the low doping ratios can prevent the concentration quenching of luminophores [22]. However, higher loading amounts per nanoparticle are necessary to achieve bright nanoparticles for specific applications [23]. In the present work, both the exciton manipulation in RUB NAs and the electrochemistry behaviors of co-reactants were mediated by a supramolecular strategy (Scheme 1). The unprecedented ECL performances in aqueous conditions were achieved, and this enables RUB NAs to be promising candidates for ECL microscopy. The proposed strategy simultaneously modulates both photophysical and electrochemical factors governing ECL, providing a versatile approach for fabricating high-performance nano-emitters.

2 | Experimental Methods

2.1 | Synthesis of Nanoparticles

The microfluidic chip is utilized in this study to achieve a rapid and stable nanoflash process through the fluid focusing structure, enabling the synthesis of nanoparticles with precise control over their size. The comprehensive manufacturing method and dimensional parameters of the microreactor can be found in Figure S1A. The fundamental principle of this microreactor hinges on the creation of a laminar flow environment featuring high flow velocity and low Reynolds number through microscale cross-flow focusing units, facilitating stable and homogeneous mixing of the organic and aqueous phases. RUB (0–2 mM), *N*,*N*'-diphenyl-*N*,*N*'-di(p-tolyl)benzidine (TPD) (0–2 mM), and DSPE-PEG2k (2 mg/mL) were solubilized in tetrahydrofuran (THF) and effectively amalgamated. The THF mixture was introduced into the organic phase inlet of the microfluidic chip via a flow rate of 5 μL/min (1 mL). Concurrently, ultrapure water was pumped into the aqueous phase inlet of the microfluidic chip at a flow rate of 100 μL/min. At the convergence point of the aqueous and organic phases within the cross-unit, the laminar flow continued steadily, coupled with rapid evaporation of the THF solvent into the aqueous phase. Consequently, hydrophobic molecules including RUB and TPD precipitated, with the hydrophobic chains of DSPE-PEG2k rapidly adsorbing onto the surface of the formed aggregates. Simultaneously, the hydrophilic terminus ensured the uniform dispersion and stability of the resulting nanoparticles within the aqueous phase.

The particle size distribution of nanoparticles was investigated by varying the total feeding amount of RUB and TPD under specific preparation conditions, with a fixed feeding ratio of 1:1 (Figure S1B). When both RUB and TPD were fed at a concentration of 1 mM, the average particle size of the resulting nanoparticles was approximately 30 nm (Figure S1C).

2.2 | Fluorescence Lifetime Fitting Models

All lifetime fits were performed in Origin 2025b using the nonlinear least-squares algorithm. Instrument response function (IRF) deconvolution was applied; fitting range 0–1000 ns; initial guesses for τ_i set based on preliminary decay profiles.

Mono-exponential decay:

$$I(t) = A_1 e^{-\frac{t}{\tau_1}} \tag{1}$$

Tri-exponential decay:

$$I(t) = A_1 e^{-\frac{t}{\tau_1}} + A_2 e^{-\frac{t}{\tau_2}} + A_3 e^{-\frac{t}{\tau_3}} \tag{2}$$

The fluorescence decay curves were fitted with mono-, bi- or tri-exponential functions. For each sample, the optimal model was selected based on the reduced chi-square (χ^2) and the randomness of residuals. Table S1 lists the fitted lifetimes (τ_i) and amplitudes (A_i).

2.3 | Measurement of Fluorescence Quantum Yield

The relative method is commonly employed for measuring fluorescence quantum yield (FLQY). Referring to the reported comparative method [22], this technique utilizes a standard sample with a known FLQY (fluorescein) and calculates the quantum yield of the sample under investigation using the following equation at the same excitation wavelength:

$$QY_s = QY_{ref}\left(\frac{F_s}{F_{ref}}\right)\left(\frac{A_{ref}(\lambda_{exc})}{A_s(\lambda_{exc})}\right)\left(\frac{n_s^2}{n_{ref}^2}\right) \tag{3}$$

Here, the subscripts **ref** and ***s*** denote the reference standard and the sample, respectively. **QY** represents the FLQY, ***F*** indicates the integrated fluorescence intensity at the excitation wavelength, ***A*** represents the absorbance at the excitation wavelength, and

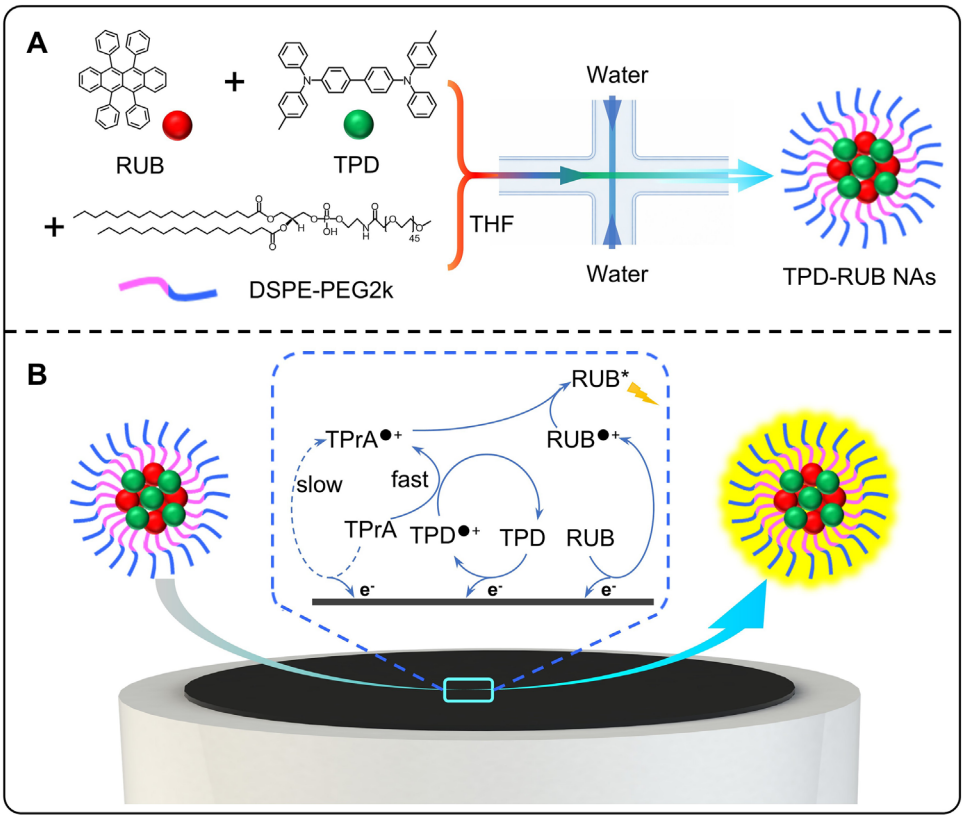

SCHEME 1 | Schematic diagram of (A) the preparation of DSPE-PEG encapsulated RUB-TPD NAs and (B) the utilization of RUB-TPD NAs as ECL luminophores (the inset shows the redox-mediating property of TPD toward the heterogeneous oxidation of TPrA on electrode).

n is the refractive index of the solvent. Both absorption and fluorescence spectra were measured using standard 10 mm quartz cuvettes. First, absorption spectra for fluorescein and samples with different compositions of NAs were collected, as shown in Figure S3A. To obtain comprehensive fluorescence data, the fluorescence spectra were recorded at an excitation wavelength of 460 nm, as illustrated in Figure S3B. The experimental results are presented in Table S2 of the manuscript.

2.4 | ECL Kinetic Imaging

ECL kinetic imaging was performed on an inverted optical microscope. The emitted light was collected through a 100× objective (NA 0.5) and detected using an Electron-Multiplying Charge-Coupled Device (EMCCD) camera (iXon Ultra 888, Andor) with an electron-multiplying gain set to 300. A three-electrode electrochemical cell was employed, comprising indium tin oxide (ITO) as the working electrode, Ag/AgCl as the reference electrode, and a platinum wire as the counter electrode. A potential of +1.0 V was applied to initiate the ECL reaction. The electrolyte consisted of PBS (pH 7.4) containing 50 mM tripropylamine (TPrA) and nanoparticles of varying composition. For kinetic measurements, an exposure time of 1 ms was used to acquire 2000 consecutive frames, and analog-to-digital (A/D) counts were recorded within a 5 × 5-pixel region. The A/D count parameters are defined as follows:

$$\frac{A}{D}Counts = \frac{N_p \times QE \times EM\ Gain}{\frac{A}{D}unit} \quad (4)$$

Here, N_p denotes the number of photons detected per pixel; QE refers to the detector's quantum efficiency; EM Gain is the camera's electron-multiplying gain, set to 300 in this study; and A/D unit represents the analog-to-digital conversion factor.

2.5 | Summary of Patterned ITO Electrode Fabrication

Patterned ITO electrodes were fabricated by standard UV photolithography. Briefly, ITO-coated glass substrates were sequentially cleaned with acetone, isopropanol, and deionized water, followed by oxygen plasma treatment to improve surface cleanliness and photoresist adhesion. A negative photoresist (SU-8 2002) was then spin-coated onto the ITO surface and soft-baked to form a uniform insulating layer. The photoresist was exposed to UV light through a photomask to define the desired microstructures, followed by development and post-baking to remove unexposed regions and stabilize the patterned structures. The resulting substrates consisted of exposed conductive ITO regions surrounded by electrically insulating photoresist, which were directly used as working electrodes for ECL imaging experiments.

3 | Results and Discussion

RUB is the most well-studied semiconductor molecule that can perform efficient TTA and also efficient reverse process SF due to the unique electronic structure (S1 ~ 2 × T1). While TTA follows a Dexter-type energy transfer mechanism, which is a short-range

process, high RUB content is required for TTA to occur. However, it has been revealed that ultrafast SF dominates over TTA in solid states of RUB, such as aggregates or films, and is the main reason for detrimental concentration quenching in these systems [24]. Decorating RUB with bulky moieties can significantly decrease SF in the solid states [25], but the alteration of electronic structure can also suppress TTA. We have demonstrated that the photophysical properties of organic molecules can be reserved in NAs by the use of a molecular matrix [22]. Also inspired by the host–guest molecular systems in the field of OLED, which are constructed in the form of solid films, we demonstrate here that SF can be diminished and TTA can be performed efficiently in a molecular matrix of hole-transporting molecules with high RUB content. Several commonly used small molecules (TPD, NPB, and CBP, the molecular structures are shown in Figure 2) with twisted geometric structures were selected as matrix molecules with the anticipation of reducing the interactions between the neighboring RUB molecules. Their hole-transporting property was also considered and discussed in ECL investigations.

Lipid-polymer (DSPE-PEG) encapsulated water-soluble NAs (Scheme 1A) were prepared according to our previous method with the assistance of microfluidic chips [22]. The component ratio of RUB with the matrix molecules and the aggregate size can easily be tailored by adjusting the injection parameters of microfluidics (Part II in Supporting Information). Typically, hybrid NAs (RUB-TPD) with a diameter of approximately 30 nm (Figure S1), composed of equivalent ratios of RUB and TPD, were prepared for investigation. In contrast to the fluorescence kinetics of RUB in organic solution, which shows a single-exponential decay law with a lifetime of ~14 ns (Figure 1A), RUB NAs either with or without the matrix molecules show multi-exponential decay profiles (Figure 1B–E). These profiles can be well fitted with a tri-exponential decay function (Table S1) [26]. The fluorescence of RUB NAs decays more rapidly (Figure 1F), and a sharply shortened fluorescence lifetime (3.2 ns) dominates the amplitude. Based on extensive research in this field, the occurrence of SF in RUB NAs can be confirmed, and this can account for the lower FLQY (13%) (Part V in Supporting Information).

With the incorporation of matrix molecules (TPD, NPB, or CBP), the fluorescence of hybrid NAs was greatly enhanced (Figure 1G). Although these hole-transporting molecules exhibit fluorescence under UV irradiation, their emission was effectively excluded by using a longer excitation wavelength (480 nm). Furthermore, the presence of matrix molecules (TPD) does not alert the absorption spectrum of RUB (Figure 1H), which precludes the ground-state electronic coupling. The fluorescence enhancement of RUB in hybrid NAs was attributed to the suppression of SF. This can be confirmed by the increase in fluorescence lifetimes of the prompt components (τ_1) (Figure 1F) and the amplitude increase of the long-lived component (τ_2) (Figure 1B–E). More importantly, the significant increase in amplitude contribution from delayed components (over 140 ns) confirms the efficient TTA (τ_3). Although the detailed exciton dynamics require further investigation, suppressing SF while maintaining TTA achieves a long-sought "sweet spot" [27], which is an optimal balance maximizing triplet exciton utilization in both electroluminescent and ECL applications, where 75% excitons are triplet (Figure 2A). Taken together, the lifetime-component evolution supports an exciton-management effect (SF suppression with TTA retained), which provides a direct photophysical rationale for the ECL enhancement discussed next.

While both SF and TTA depend on intermolecular coupling, it has been demonstrated that the separation of RUB molecules by increasing the intermolecular distance or by molecular spacers can attain the optimum intermolecular coupling [28, 29]. Given the comparable molecular sizes of three matrix molecules (TPD, NPB, and CBP), the differences in their electronic structures should account for the performances in suppressing SF. Since LUMO are hopping sites for electron transfer, the high lied LUMO of spacing molecules leads to an energy barrier (ΔE_{LUMO}) for intermolecular electron transfer [29]. According to this rule, TPD with a very high LUMO level can afford effective electronic effects on the suppression of RUB SF (Figure 2B), and shows the best performance. NPB and CBP with relatively lower LUMO levels exhibit inferior SF suppression capabilities compared to TPD. For further contrast, the SF suppression capability of an electron-transporting molecule, Alq3, with an even lower LUMO level was investigated (Figure S2). Consequently, it depresses the fluorescence emission of RUB. These comparisons indicate the important role of a high-lying LUMO level in improving the photophysical properties of RUB. Due to its outstanding performance (about 2.3-fold at the equivalent mole ratio, FLQY = 30%), TPD was mainly discussed in the following ECL investigations.

RUB can generate ECL via both annihilation-type ($RUB^+ + RUB^- \rightarrow RUB^*$) and co-reactant pathways in organic solutions. Since the reduction potential of RUB lies beyond the electrochemical window of water (Figure S4), the co-reactant pathway is preferred in aqueous solutions [30]. TPrA was employed as an oxidation–reduction co-reactant, whose oxidative decomposition generates strong reducing intermediates that subsequently undergo ion annihilation with RUB cations to produce excited states (Mechanism I). As shown in Figure 2C, RUB NAs show only weak ECL signals under anodic potential scans. After the incorporation of TPD into RUB NAs, greatly enhanced ECL signals and a more negative peak potential were achieved (0.97 V). The negatively shifted peak potential enables us to achieve a maximum ECL signal at a lower potential within the electrochemical window of water (Figure 2D). About a 50-fold signal enhancement was obtained. The ECL spectrum of RUB-TPD NAs matches well with the fluorescence spectrum of RUB (Figure 2E). This indicates that RUB acted as the ECL luminophore and that the emission was from the excited singlet states, which formed either from direct population or from TTA (Figure 2A). The mediated photophysical properties discussed above undoubtedly constitute the fundamental basis for the improved ECL performance. Below, we demonstrate that the electrochemical properties of TPD also play an important role in improving the ECL behavior of RUB NAs.

Mechanism I

$$RUB - e^- \rightarrow RUB^{\bullet+} \quad (5)$$

$$TPrA - e^- \rightarrow TPrA^{\bullet+} \quad (6)$$

$$TPrA^{\bullet+} - H^+ \rightarrow TPrA^{\bullet} \quad (7)$$

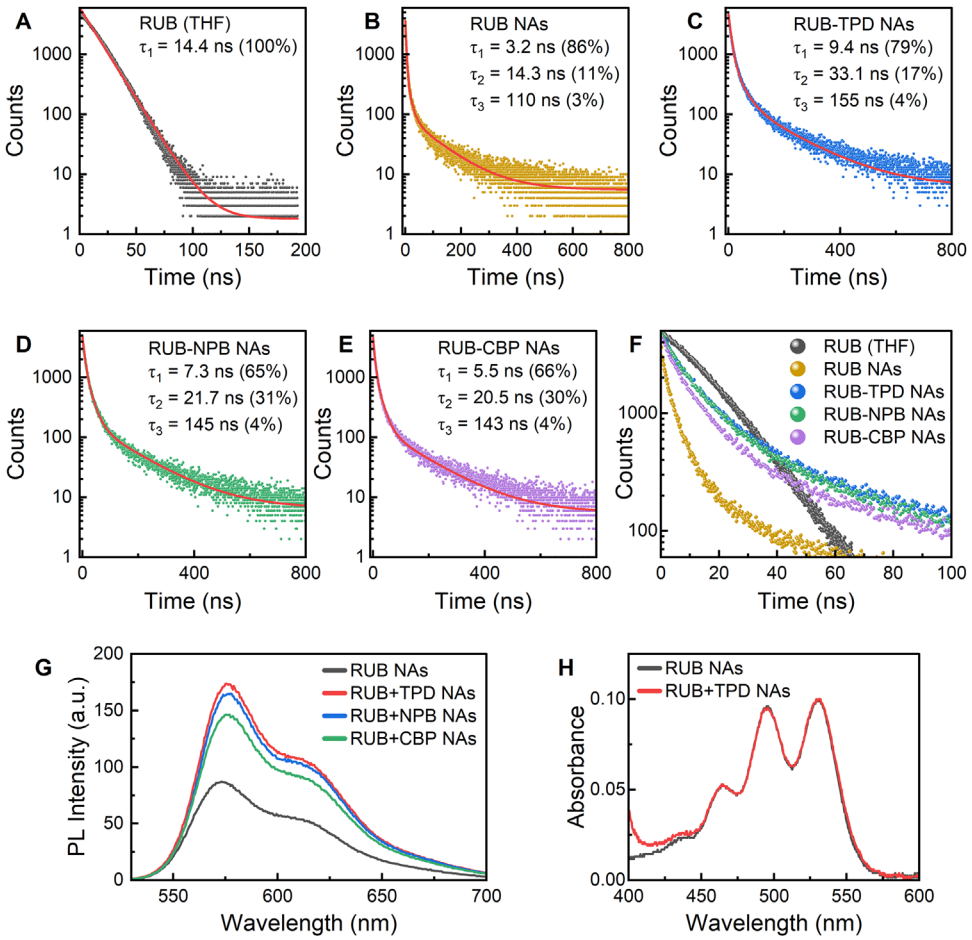

FIGURE 1 | Time-resolved fluorescence decay curves of (A) RUB in THF, (B) RUB NAs, (C) RUB-TPD NAs, (D) RUB-NPB NAs, and (E) RUB-CBP NAs. The fluorescence lifetime and amplitude weight of the components were included. (F) The comparison of RUB and hybrid NAs to show the decay change of prompt components. (G) Steady-state fluorescence emission spectra of RUB and hybrid NAs. (H) UV-vis absorption spectra of RUB NAs and RUB-TPD NAs.

$$RUB^{\bullet+} + TPrA^{\bullet} \rightarrow RUB^{*} + TPrA_{OX} \quad (8)$$

Mechanism II

$$TPD - e^{-} \rightarrow TPD^{\bullet+} \quad (9)$$

$$RUB - e^{-} \rightarrow RUB^{\bullet+} \quad (10)$$

$$(RUB^{\bullet+} + TPrA \rightarrow RUB + TPrA^{\bullet+}) \quad (11)$$

$$TPD^{\bullet+} + TPrA \rightarrow TPD + TPrA^{\bullet+} \quad (12)$$

$$TPrA^{\bullet+} - H^{+} \rightarrow TPrA^{\bullet} \quad (13)$$

$$RUB^{\bullet+} + TPrA^{\bullet} \rightarrow RUB^{*} + TPrA_{OX} \quad (14)$$

The redox-mediating capability of TPD can be confirmed by the investigation of ECL in organic solutions, where there is no concentration quenching or exciton manipulation for RUB [31]. Under broader potential ranges, RUB undergoes two successive one-electron oxidative processes, and the second oxidation–reduction process is less reversible (Figure 3A). In contrast, the cyclic voltammetry of RUB is more reversible under narrower potential ranges (Figure 3B). From the ECL-potential profiles of RUB (Figure 3E), a maximum ECL signal was produced at 1.24 V. The presence of TPD in RUB solutions can obviously enhance the ECL intensity, and the peak potential becomes more negative gradually with the increasing of TPD concentration (Figure 3E). The maximum ECL intensity was achieved with an equivalent mole ratio of RUB/TPD. Due to the TPD-induced negative shift of ECL peak potential, an obviously enhanced ECL signal (2.8-fold) can be achieved at lower potentials (Figure 3F). Notably, the CV of the RUB/TPD mixture shows no new redox features and largely resembles the superposition of the individual components (Figure S5), suggesting no appreciable side reaction between oxidized TPD and RUB under the tested conditions.

The low oxidation potential of TPD and the high oxidation capability of TPD radical cation can account for the shifting of luminescent potential and enhancement of ECL intensity. As indicated in Mechanism I, the oxidation of co-reactant TPrA is a key step to produce strong reducing intermediates. Due to the irreversibility and slow dynamics of the heterogeneous oxidation of TPrA on electrodes [32], more positive oxidation potential and larger TPrA concentrations are always used to achieve higher ECL efficiency. The oxidation of TPrA can also be achieved homogeneously by the oxidation products of luminophores, which are the origin of complex mechanisms for co-reactant pathways but also enable homogeneous redox mediation [33, 34]. The disappearance of the reduction wave of RUB in the presence of TPrA (Figure 3B) indicates the homogeneous reactions

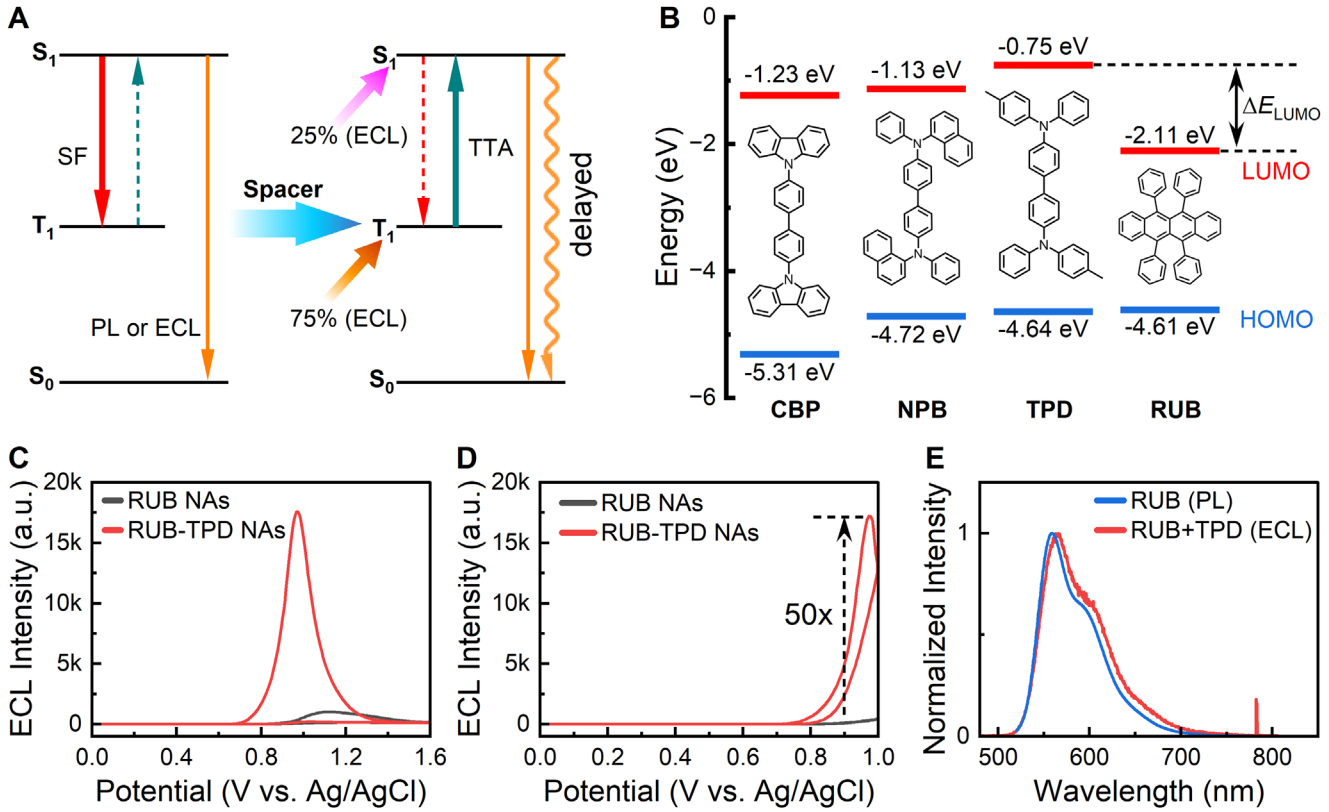

FIGURE 2 | (A) Physical model showing the change in exciton formation states before (SF dominates) and after (TTA dominates) the inclusion of a molecular spacer. (B) Energy diagram showing the energy levels of related molecules and the energy barrier of LUMO. (C and D) The ECL-potential profiles of RUB NAs and RUB-TPD NAs in aqueous solutions (0.1 M PBS, pH = 7.4, 10 mM TPrA) under different CV potential ranges. (E) Fluorescence spectrum of RUB in THF and ECL spectrum of TPD-RUB NAs.

(Equation 11 in Mechanism II). TPD features two quasi-reversible oxidation–reduction processes during anodic potential scanning and more negative oxidation potentials than RUB (Figure 3C). The homogeneous reaction of TPD radical cations with TPrA can also be confirmed by the decrease or disappearance of the TPD reduction wave (Figure 3D). The results of density functional theory (DFT) calculations can also support the oxidation ability of RUB and TPD radical cation toward neutral TPrA (Figures 3G and S6). The low-lying singly occupied molecular orbital (SOMO) forms a quasi-closed-shell electronic configuration (Figure 3G), which can account for the well-known stability of TPD radical cation [35]. The unoccupied spin counterpart (SUMO) is deep enough to receive an electron from the HOMO of neutral TPrA, confirming the homogeneous oxidation or hole-transporting ability toward TPrA (Equation 12 in Mechanism II).

In view of the slow dynamics of the heterogeneous oxidation of TPrA on electrode [32], different hole-transporting rates toward TPrA should exist between RUB and TPD. This can be confirmed directly from the differences of their corresponding empty molecular orbitals that can accept electrons from the HOMO of TPrA (Figures 3G and S6). There are two orbitals can accept electrons for RUB, but there is only one orbital can accept electrons from TPrA for TPD. While these reactions follow an outer-sphere electron transfer mechanism [36], the Marcus theory of electron transfer is adopted to investigate the hole-transporting rate between molecules [37]. According to this theory, the electronic coupling (V) and the reorganization energy (λ) are the key parameters to determine the hole-hopping rate (k_{hole}) (Equation 15). The reorganization energy includes internal reorganization energy (λ_{in}) and external reorganization energy (λ_{out}) [38]. The λ_{in} reflects the changes of molecular geometry and was mainly considered in the well-exploited applications as solid states [39]. While the λ_{out} in condensed phases is much smaller than λ_{in} and is always neglected [40, 41], solvent reorganization energy cannot be ignored in solutions considering the charged states of radicals and the electronic polarization of the surrounding medium [42]. According to the calculation results (Table S3), λ_{out} gives much more contribution to the total reorganization energy λ_{tot} and actually determines the hole-transporting rates. A smaller λ_{tot} and much larger k_{hole} were obtained for TPD radicals compared with that of RUB radicals toward TPrA. The ECL enhancement in organic solution by TPD inclusion can be explained by the differences of hole-transporting capability between RUB and TPD. In addition, the oxidation potential of TPD is more negative and the TPD radicals are more stable than that of RUB, the generated RUB radicals can only account for the ion annihilation and produce more ECL (Mechanism II). The redox-mediating capability of TPD toward TPrA can be well reserved in RUB-TPD NAs, and higher ECL efficiency can be achieved in aqueous solutions with a relatively low TPrA concentration.

$$k_{hole} = \left(\frac{\pi}{\lambda k_b T}\right)^{\frac{1}{2}} \frac{V^2}{h} \exp\left(-\frac{\lambda}{4k_b}\right) \quad (15)$$

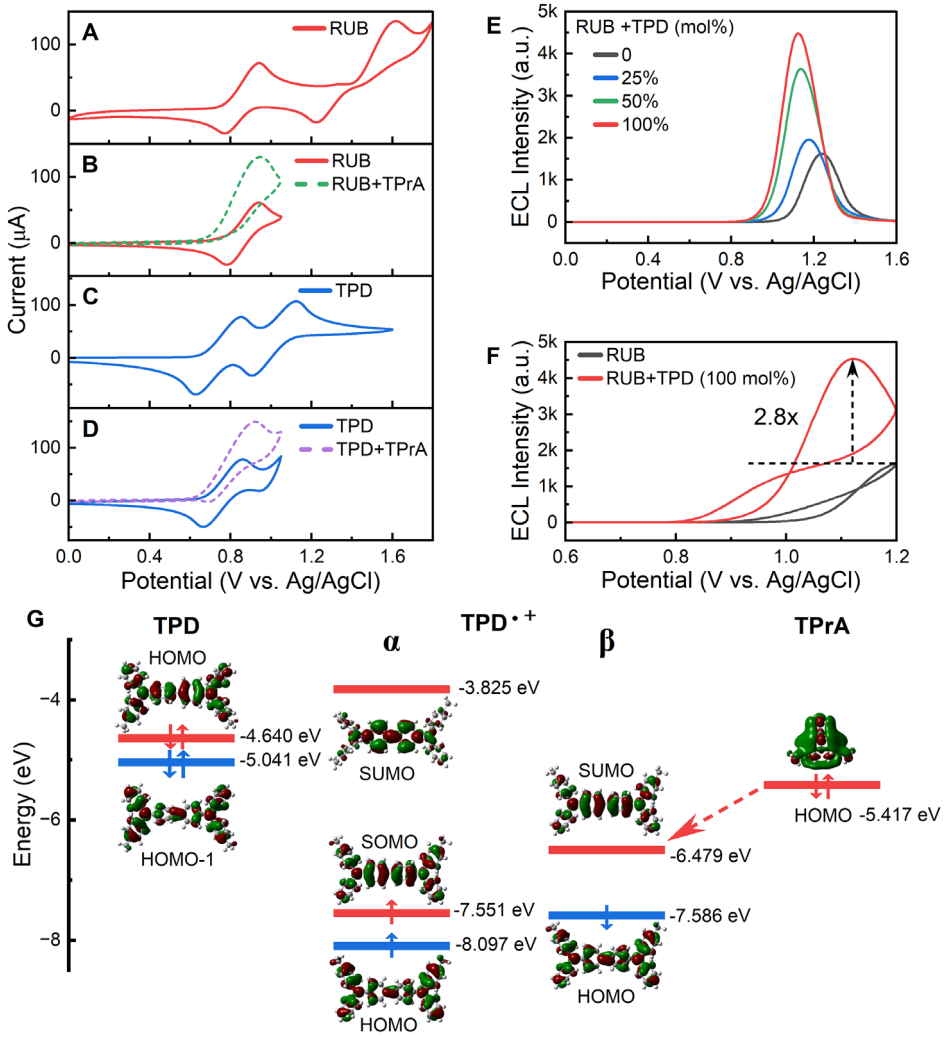

FIGURE 3 | (A) CV of RUB (1 mM) in CH_2Cl_2 recorded under a wide potential region. (B) CV of RUB (1 mM) and RUB (1 mM) + TPrA (1 mM) under a narrow potential region. (C) CV of TPD (1 mM) in CH_2Cl_2 recorded under a wide potential region. (D) CV of TPD (1 mM) and TPD (1 mM) + TPrA (1 mM) under a narrow potential region. (E) ECL-potential curves of RUB (1 mM) with varying TPD concentrations in CH_2Cl_2. (F) Comparison of ECL-potential profiles for RUB and RUB + TPD under a narrow potential window. (G) DFT-calculated molecular orbitals with corresponding energy levels, illustrating the electron transfer from TPrA to the TPD cation.

The development of high-efficiency ECL luminophores as aqueous imaging probes has shown significant promise, particularly when coupled with advanced detection systems offering spatiotemporal high-resolution capabilities. The single-molecule electrochemical events of $[Ru(bpy)_3]^{2+}$ have been discerned from their ECL signals by an EMCCD-based imaging equipment [2]. In the present work, the discrete photon signals acquired at similar equipment were used to demonstrate the imaging capability of RUB-TPD NAs. Compared with the single-photon discrete signals of $[Ru(bpy)_3]^{2+}$ (Figure 4A,B), multi-photon signals were obtained under the same exposure conditions for RUB-TPD NAs (Figure 4D,E). Notably, the burst amplitude and occurrence frequency increased with the TPD fraction under identical acquisition conditions, supporting the mediator-enhanced ECL performance of the hybrid Nas (Part VIII Figure S7 in Supporting Information).

The RUB-TPD NAs were used as ECL imaging probes and the performances were investigated by the imaging of patterned microelectrode arrays. Both $[Ru(bpy)_3]^{2+}$ and RUB-TPD NAs were employed as homogeneous imaging probes in these experiments, and the patterned electrodes were used to spatially define the ECL emission. With a low operating potential (1.0 V), the obtained imaging patterns matched well with the fabricated microstructures. Based on the mediated ECL performances, the RUB-TPD NAs outperformed the well-exploited $[Ru(bpy)_3]^{2+}$ in reproducing the pattern details (Figure 4C,F). The RUB-TPD NAs with competitive ECL imaging performances under physiologically compatible operating conditions especially under lower potentials may find wide applications in bioimaging and bioanalysis.

4 | Conclusion

Semiconducting charge transport and redox activity are the two notable features of triphenylamine-based organic radicals, and have widely exploited in separated applications, such as OLEDs and organic electrosynthesis. The integration of these features

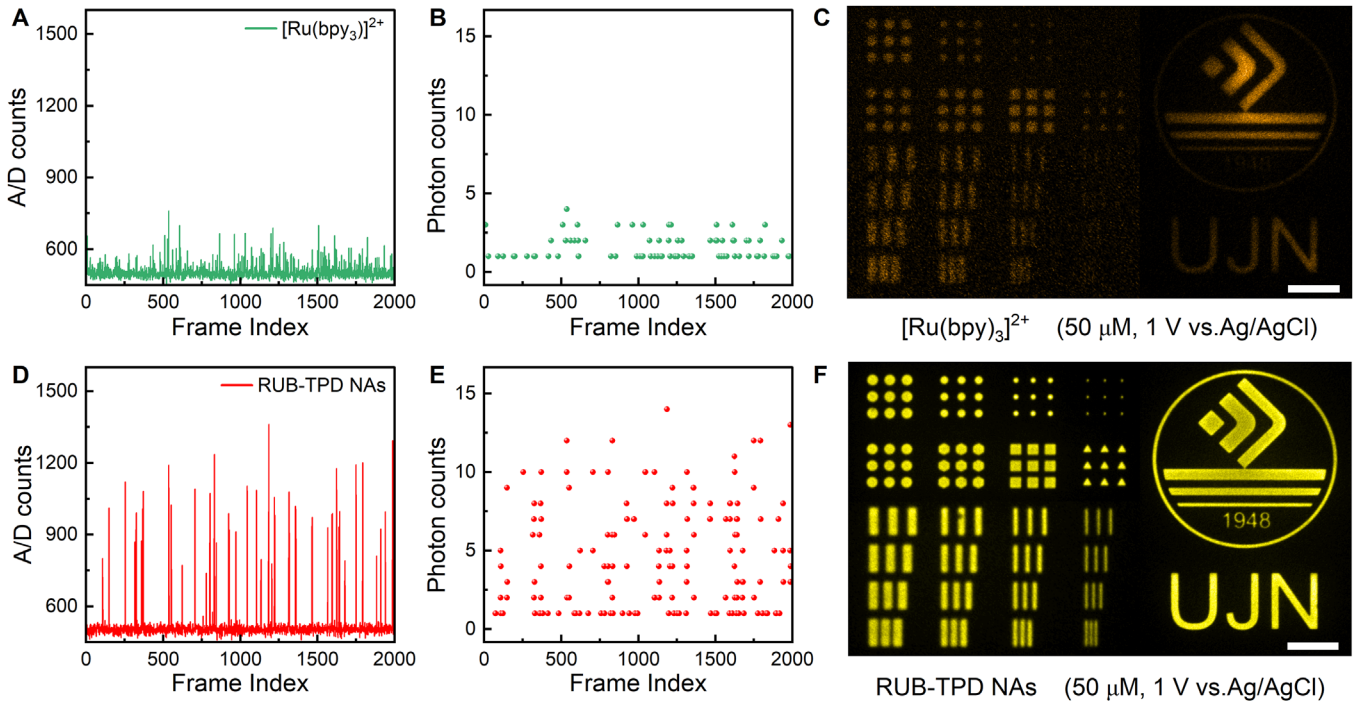

FIGURE 4 | The discrete photon signals and the calculated photon numbers of each event of (A and B) $[Ru(bpy)_3]^{2+}$ and (D and E) TPD-RUB NAs acquired from a single pixel of the EMCCD. Exposure time, 1 ms. Comparison of ECL imaging performance on ITO patterned arrays using (C) $[Ru(bpy)_3]^{2+}$ and (F) TPD-RUB NAs at an applied potential of 1.0 V in the presence of 50 mM TPrA. Scale bar: 200 μm.

and beyond in the present work showcases unprecedented ECL applications and exciting results. The exploitation of hole-transporting molecules as ECL mediators for different types of luminophores can build up a universal strategy. However, the unique molecular structure and its own excellent property of RUB, such as pronounced hole mobility, cannot be overlooked for these achievements. Some criteria for the matching of ECL mediators and luminophores need to be established for universal applications. The TPD-mediated RUB NAs deserve to be a benchmark system for evaluating anodic ECL behaviors. The revolutionized ECL behaviors in aqueous conditions show promising potential in the fields of biosensing, new light-emitting devices, and other applications.

Author Contributions

Li Dai: methodology, investigation, writing – original draft. **Tong Jiang**: investigation. **Baotao Kang**: validation. **Yu Du**: validation. **Zhongfeng Gao**: validation. **Xiang Ren**: writing – review and editing. **Dan Wu**: writing – review and editing. **Hongmin Ma**: conceptualization, methodology, writing – original draft, funding acquisition. **Qin Wei**: resources, funding acquisition, supervision. **Huangxian Ju**: validation, resources, supervision.

Acknowledgments

This work was financially supported by the National Natural Science Foundation of China (22374059 and 22274062). Hongmin Ma thanks the Young Taishan Scholars Program of Shandong Province of China.

Conflicts of Interest

The authors declare no conflicts of interest.

References

1. Y. Wang, J. Ding, P. Zhou, et al., "Electrochemiluminescence Distance and Reactivity of Coreactants Determine the Sensitivity of Bead-Based Immunoassays," *Angewandte Chemie International Edition* 62 (2023): e202216525.

2. J. Dong, Y. Lu, Y. Xu, et al., "Direct Imaging of Single-Molecule Electrochemical Reactions in Solution," *Nature* 596 (2021): 244–249.

3. S. Knezevic, D. Han, B. Liu, D. Jiang, and N. Sojic, "Electrochemiluminescence Microscopy," *Angewandte Chemie International Edition* 63 (2024): e202407588.

4. Y. Zhao, L. Bouffier, G. Xu, G. Loget, and N. Sojic, "Electrochemiluminescence With Semiconductor Nanomaterials," *Chemical Science* 13 (2022): 2528–2550.

5. S. O'Connor, L. Dennany, and E. O'Reilly, "Evolution of Nanomaterial Electrochemiluminescence Luminophores Towards Biocompatible Materials," *Biosensors & Bioelectronics* 149 (2023): 108286.

6. R. Luo, H. Lv, Q. Liao, et al., "Intrareticular Charge Transfer Regulated Electrochemiluminescence of Donor-Acceptor Covalent Organic Frameworks," *Nature Communications* 12 (2021): 6808.

7. B. Yin, L. Jiang, X. Wang, et al., "Bright Dual-Color Electrochemiluminescence of a Structurally Determined Pt_1Ag_{18} Nanocluster," *Aggregate* 5 (2024): e417.

8. E. Kerr, S. Knezevic, P. S. Francis, et al., "Electrochemiluminescence Amplification in Bead-Based Assays Induced by a Freely Diffusing Iridium(III) Complex," *ACS Sensors* 8 (2023): 933–939.

9. M. Liu, X. Huang, B. Goudeau, C. Wang, N. Sojic, and H. Li, "Electrochemiluminescence Modulation by a Versatile Organic Redox Mediator," *Angewandte Chemie International Edition* 64 (2025): e20178.

10. W. Miao, "Electrogenerated Chemiluminescence and Its Biorelated Applications," *Chemical Reviews* 108 (2008): 2506–2553.

11. K. Chu, Z. Ding, and E. Zysman-Colman, "Materials for Electrochemiluminescence: TADF, Hydrogen-Bonding, and Aggregation- and

Crystallization-Induced Emission Luminophores," *Chemistry – A European Journal* 29 (2023): e202301504.

12. R. Ishimatsu, S. Matsunami, T. Kasahara, et al., "Electrogenerated Chemiluminescence of Donor-Acceptor Molecules With Thermally Activated Delayed Fluorescence," *Angewandte Chemie International Edition* 53 (2014): 6993–6996.

13. E. M. Gross, N. R. Armstrong, and R. M. Wightman, "Electrogenerated Chemiluminescence From Phosphorescent Molecules Used in Organic Light-Emitting Diodes," *Journal of the Electrochemical Society* 149 (2002): E137–E142.

14. B. Zhang, Y. Kong, H. Liu, et al., "Aggregation-Induced Delayed Fluorescence Luminogens: The Innovation of Purely Organic Emitters for Aqueous Electrochemiluminescence," *Chemical Science* 12 (2021): 13283–13291.

15. H. Gao, S. Y. Shi, S. M. Wang, et al., "Aggregation-Induced Delayed Electrochemiluminescence of Organic Dots in Aqueous Media," *Aggregate* 5 (2024): e394.

16. R. Ishimatsu, Y. Kirino, C. Adachi, K. Nakano, and T. Imato, "Quenching Behavior of Thermally Activated Delayed Fluorescence From a Donor–Acceptor Molecule, 1,2,3,5-Tetrakis(Carbazol-9-yl)-4,6-Dicyanobenzene by O_2," *Chemistry Letters* 45 (2016): 1183–1185.

17. L. Huang, T. Le, K. Huang, and G. Han, "Enzymatic Enhancing of Triplet-Triplet Annihilation Upconversion by Breaking Oxygen Quenching for Background-Free Biological Sensing," *Nature Communications* 12 (2021): 1898.

18. D. Di, L. Yang, J. M. Richter, et al., "Efficient Triplet Exciton Fusion in Molecularly Doped Polymer Light-Emitting Diodes," *Advanced Materials* 29 (2017): 1605987.

19. E. Radiunas, L. Naimovičius, P. Baronas, A. Jozeliūnaitė, E. Orentas, and K. Kazlauskas, "CN-Tuning: A Pathway to Suppress Singlet Fission and Amplify Triplet-Triplet Annihilation Upconversion in Rubrene," *Advanced Optical Materials* 13 (2025): 12.

20. J. T. Maloy and A. J. Bard, "Electrogenerated Chemiluminescence. VI. Studies of the Efficiency and Mechanisms of 9,10-Diphenylanthracene, Rubrene, and Pyrene Systems at a Rotating-Ring-Disk Electrode," *Journal of the American Chemical Society* 93 (1971): 5968–5981.

21. K. M. Omer and A. J. Bard, "Electrogenerated Chemiluminescence of Aromatic Hydrocarbon Nanoparticles in an Aqueous Solution," *Journal of Physical Chemistry C* 113 (2009): 11575–11578.

22. L. Dai, J. Fang, T. Jiang, et al., "Multicomponent Supramolecular Nanoaggregates With Co-Emissive Electrochemiluminescence," *Matter* 8 (2025): 102056.

23. N. S. Adamson, S. J. Blom, E. H. Doeven, et al., "Electrochemiluminescence Enhanced by a Non-Emissive Dual Redox Mediator," *Angewandte Chemie International Edition* 63 (2024): e202412097.

24. P.-H. Sher, C.-H. Chen, T.-L. Chiu, C.-F. Lin, J.-K. Wang, and J.-H. Lee, "Distinct Routes of Singlet Fission and Triplet Fusion: A Fluorescence Kinetic Study of Rubrene," *Journal of Physical Chemistry C* 123 (2019): 3279–3284.

25. E. Radiunas, M. Dapkevicius, S. Raisys, et al., "Impact of t-Butyl Substitution in a Rubrene Emitter for Solid State NIR-to-Visible Photon Upconversion," *Physical Chemistry Chemical Physics* 22 (2020): 7392–7403.

26. E. Radiunas, M. Dapkevicius, S. Raisys, and K. Kazlauskas, "Triplet and Singlet Exciton Diffusion in Disordered Rubrene Films: Implications for Photon Upconversion," *Physical Chemistry Chemical Physics* 24 (2022): 24345–24352.

27. P. Baronas, G. Kreiza, L. Naimovicius, et al., "Sweet Spot of Intermolecular Coupling in Crystalline Rubrene: Intermolecular Separation to Minimize Singlet Fission and Retain Triplet-Triplet Annihilation," *Journal of Physical Chemistry C* 126 (2022): 15327–15335.

28. W. Jia, Q. Chen, L. Chen, et al., "Molecular Spacing Modulated Conversion of Singlet Fission to Triplet Fusion in Rubrene-Based Organic Light-Emitting Diodes at Ambient Temperature," *Journal of Physical Chemistry C* 120 (2016): 8380–8386.

29. X. Tian, L. Zhou, X. Chen, et al., "Nanoscale Exponential Distance Dependence and Electron-Transfer Model for Intermolecular Singlet Exciton Fission Observed in Rubrene-Doped Organic Films," *Organic Electronics* 50 (2017): 429–434.

30. J. E. Dick, C. Renault, B. K. Kim, and A. J. Bard, "Electrogenerated Chemiluminescence of Common Organic Luminophores in Water Using an Emulsion System," *Journal of the American Chemical Society* 136 (2014): 13546–13549.

31. S. Knežević, E. Kerr, G. Valenti, et al., "Electrocatalytic Amplification of Coreactant Electrochemiluminescence Using Redox Mediators," *Electrochimica Acta* 499 (2024): 144677.

32. R. Y. Lai and A. J. Bard, "Electrogenerated Chemiluminescence. 70. The Application of ECL to Determine Electrode Potentials of Tri-*n*-Propylamine, Its Radical Cation, and Intermediate Free Radical in MeCN/Benzene Solutions," *Journal of Physical Chemistry A* 107 (2003): 3335–3340.

33. E. Kerr, D. J. Hayne, L. C. Soulsby, et al., "A Redox-Mediator Pathway for Enhanced Multi-Colour Electrochemiluminescence in Aqueous Solution," *Chemical Science* 13 (2022): 469–477.

34. A. Fracassa, C. I. Santo, E. Kerr, et al., "Redox-Mediated Electrochemiluminescence Enhancement for Bead-Based Immunoassay," *Chemical Science* 15 (2024): 1150–1158.

35. P. J. Low, M. A. J. Paterson, A. E. Goeta, et al., "The Molecular Structures and Electrochemical Response of "Twisted" Tetra(Aryl)Benzidenes," *Journal of Materials Chemistry* 14 (2004): 2516–2523.

36. F. Kanoufi and A. J. Bard, "Electrogenerated Chemiluminescence. 65. An Investigation of the Oxidation of Oxalate by Tris(Polypyridine) Ruthenium Complexes and the Effect of the Electrochemical Steps on the Emission Intensity," *Journal of Physical Chemistry B* 103 (1999): 10469–10480.

37. G. R. Hutchison, M. A. Ratner, and T. J. Marks, "Hopping Transport in Conductive Heterocyclic Oligomers: Reorganization Energies and Substituent Effects," *Journal of the American Chemical Society* 127 (2005): 2339–2350.

38. D. P. McMahon and A. Troisi, "Evaluation of the External Reorganization Energy of Polyacenes," *Journal of Physical Chemistry Letters* 1 (2010): 941–946.

39. S. Luo, B. Zheng, and S. Dong, "Natural Light-Regulated Switchable Self-Adhesive Supramolecular Films for Smart Windows," *Chemistry – A European Journal* 29 (2023): e202301277.

40. L.-F. Ji, J.-X. Fan, G.-Y. Qin, N.-X. Zhang, P.-P. Lin, and A.-M. Ren, "Theoretical Study on the Electronic Structures and Charge Transport Properties of a Series of Rubrene Derivatives," *Journal of Physical Chemistry C* 122 (2018): 21226–21238.

41. R. Herzhoff, F. Negri, K. Meerholz, and D. Fazzi, "Revealing the Interplay Between the Structural Complexity of Triphenylamine Redox Derivatives and Their Charge Transport Processes via Computational Modeling," *Journal of Materials Chemistry C* 11 (2023): 11969–11979.

42. V. Vaissier, P. Barnes, J. Kirkpatrick, and J. Nelson, "Influence of Polar Medium on the Reorganization Energy of Charge Transfer Between Dyes in a Dye Sensitized Film," *Physical Chemistry Chemical Physics* 15 (2013): 4804–4814.

Supporting Information

Additional supporting information can be found online in the Supporting Information section.

Supporting File: agt270315-sup-0001-SuppMat.docx.